Journal of Sustainable Metallurgy (2022) 8:1026–1040
https://doi.org/10.1007/s40831-022-00545-5

RESEARCH ARTICLE

Recovery of Cu and Ni in Electroplating Sludge by a Low-Temperature Alkaline Smelting Technique

Hui Xiao[1] · Peng Chen[1] · Lin Chen[1] · Duchao Zhang[1] · Weifeng Liu[1] · Tianzu Yang[1]

Received: 7 January 2022 / Accepted: 7 May 2022 / Published online: 2 June 2022

Abstract

Serious concerns have been raised from the solid waste processing field about minimizing the environmental footprint of electroplating sludge (ES), not only because of its hazardousness but also due to the rising demand for recycling non-renewable metal resources. A low-temperature alkaline matte smelting process is proposed in the present study. Na_2CO_3 was used as a flux reagent for smelting ES at 1250 °C, which is 100–250 °C lower than those previously reported. XRD and SEM–EDS revealed that the presence of Na species in the matte and slag phases was conducive to reducing the smelting temperature. The relationship between the processing parameters, i.e., Na_2CO_3, coal powder, and sulfur dosages, and the partitioning of Cu, Ni, and Cr were investigated for optimal metal recovery. A copper–nickel matte (Cu + Ni = 46.9 wt%) was produced. Cu and Ni recovery achieved 95% and 90%, respectively, while over 99% Cr was concentrated in the slag. The TCLP test indicated that heavy metal leaching toxicities of the slag were below the Chinese national identification standards (GB5085.3-2007) due to the formation of stable spinel phases and embedment of heavy metals in the glassy slag matrix.

Graphical Abstract

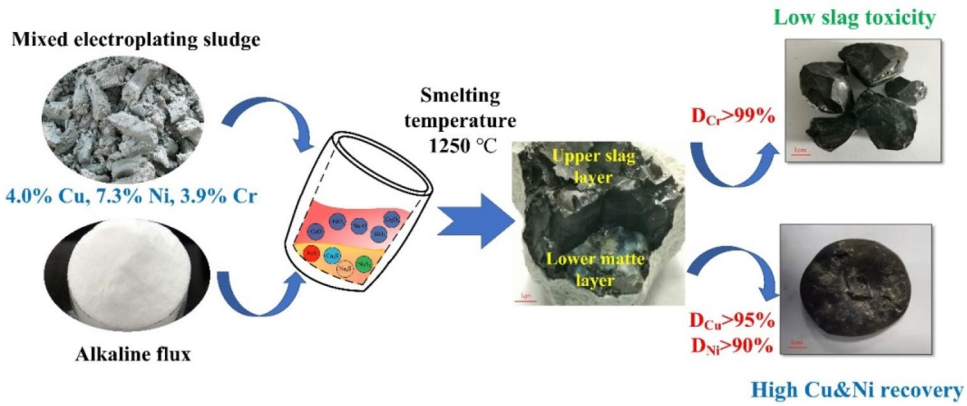

Keywords Electroplating sludge · Alkaline smelting · Cu and Ni recovery · TCLP

Introduction

The electroplating process is widely applied in various manufacturing industries, such as automobiles, electronics, metal finishing, etc., but leads to massive electroplating sludge (ES) disposal [1]. ES produced in China amounts to several million tons annually and is characterized by complex composition, strong migration ability, and severe ecological

The contributing editor for this article was Sharif Jahanshahi.

✉ Lin Chen
chenlin0210@csu.edu.cn

[1] School of Metallurgy and Environment, Central South University, Changsha 410083, China

toxicity [2], which is a high-risk threat to the ecological environment [3]. Therefore, serious concerns from both legislation and industry are raised to minimize the environmental footprint of ES, not only because of its hazardousness but also due to the rising demand for sustainable use of non-renewable metal resources [4].

Generally, 3R rules, namely, remediation, reduction, and recycling, should be considered when processing solid wastes. The solidification/stabilization method is the most widely applied technique for safe ES disposal due to its simplicity and low cost. Using a stabilization agent and/or a high-temperature calcination method [5], heavy metals can be stabilized in the matrix of fire clay brick, ceramics, or backfill materials [6–8]. However, the metal values in ES can no longer be extracted from the stabilized products, except for the volatile elements or compounds [9]. Hydrometallurgical methods were also proposed due to their ability to extract metals from ES with high recovery [10]. Typically, ES was leached by sulfuric acid, hydrochloric acid, or ammonium hydroxide solution, with subsequent precipitation, solvent extraction, or electrowinning steps for further separation/purification of various metals [1, 11, 12]. Value-added materials also can be synthesized from the leaching solution to enhance the economic feasibility of the processes [13–15]. Nevertheless, secondary pollution of leaching residues and wastewater remains challenging [2].

Recently, high-temperature smelting processes attracted great interest in extracting valuable metals from ES [16]. Tian et al. [17] reported a carbon thermal reduction and low-carbon reduction refining process for Cu ES, by which 96% Cu and 85% Ni were enriched in an anode copper plate, while 90.77% Pb, 95.14% Sn, and 99.92% Zn were recovered in the flue dust. This technique showed a high potential for industrial application because not only metal values were efficiently recovered, but also the final slag can be safely used as a construction material [18]. However, Cr is a refractory element and its content in ES usually ranges from 1.5 to 15 wt% [1], resulting in high smelting temperatures of ES. Zhou et al. [19] reported that smelting an ES with a Cr content of 6 wt% at 1500 °C using starch as the reductive agent. Zhang et al. [20] also found that an ES containing 4 wt% Cr should be smelted at a temperature above 1350 °C. Moreover, these high-temperature reductive smelting methods resulted in the formation of metal alloys to which Cu, Ni, Fe, and Cr were simultaneously reported, leading to difficulties in further purification [21, 22]. Therefore, developing a smelting technique for ES at a typical nonferrous metal smelting temperature (1000–1300 °C) would save energy and benefit further metal purification, finally leading to lower carbon emissions and sustainability of the industry.

The alkaline smelting process, in which alkaline fluxes such as Na_2CO_3, NaOH, etc. are used as flux [23], is a low-temperature smelting method for various raw materials [24]. It was reported that the smelting temperatures of Sb concentrate and waste lead paste were reduced from 1200 to 1000 °C [25] and 1350 to 880 °C [26], respectively, using alkaline smelting techniques. Meanwhile, the reaction between alkaline flux and sulfur led to the formation of a low melting point Na_2S in the matte, which facilitated phase separation during smelting [27]. Dang et al. [28] pointed out that Na_2CO_3 can also react with Cr_2O_3 to form the low melting point compound Na_2CrO_4, as shown by Eq. (1).

$$Cr_2O_3 + 2Na_2CO_3 + 1.5O_2 = 2Na_2CrO_4 + 2CO_2 \quad \Delta G^{\Theta} = -252.756\ \text{kJ/mol}. \tag{1}$$

Therefore, the alkaline smelting method showed a high potential to fill the gap between the current ES recycling technique and the need to extract metal values based on the 3R rules. However, the relationship between the element partitioning and smelting parameters needs to be extrapolated considering a possible industrial application. Concerns about the toxicity of the alkaline smelting products to the ecological system should also be addressed. In this work, alkaline smelting of ES was studied using Na_2CO_3 as the alkaline flux. The effect of Na_2CO_3 dosage, coal dosage, sulfur dosage, and FeO/SiO_2 and CaO/SiO_2 weight ratios on the partitioning of typical heavy metals, i.e., Cu, Ni and Cr, in the products was investigated. The phase and toxicity of the smelting slag were analyzed. This work suggests a low-temperature smelting route for processing ES, which will facilitate the development of harmless processing techniques for recycling abundant heavy metal-containing sludges.

Experimental

Raw Material

The raw material in this work was ES provided by Zhejiang Taitong Renewable Resources Utilization Co., Ltd., China. The ES was dried, ground, and sieved at 200 mesh to ensure homogeneity. The composition of the ES was analyzed by an X-ray fluorescence spectrometer (XRF), and metals of interest, i.e., Cu, Ni and Cr, were analyzed by inductively coupled plasma-atomic emission spectroscopy (ICP-AES). The results are listed in Table 1, showing that the mass contents of Cu, Ni, and Cr were 4.0%, 7.3%, and 3.9%, respectively. XRD analysis indicated that the ES was mainly amorphous, with only characteristic peaks of $CaSO_4$, $CaCO_3$, and SiO_2, as shown in Fig. S1 (see Supplementary File), because it was a chemical deposition from electroplating wastewater.

Table 1 Composition of the ES (dry base, wt%)

Element	Cu*	Ni*	Cr*	Fe	Zn	Pb	Na	Ca	Al	Si	S
Content (%)	4.0	7.3	3.9	20.7	3.5	0.5	1.2	10.2	2.0	2.2	2.9

*Analyzed by ICP-AES

Alkaline Smelting Experiment

According to the composition of raw ES, the FeO_x–CaO–SiO_2 slag system, which is frequently used in nonferrous metal smelting processes, was chosen in this work. The slag composition can be adjusted to obtain a melting point between 1200 and 1250 °C by adding an appropriate amount of flux according to the FeO_x–CaO–SiO_2 ternary [29]. Therefore, 1250 °C was used as the smelting temperature in the study, which is also a typical smelting temperature in copper pyrometallurgical processes [30]. A schematic diagram of the alkaline smelting procedure is illustrated in Fig. S2. The ES (50 g) was mixed with certain amounts of Fe_2O_3 (99.0%, Tianjin Kemiou Chemical Reagent Co., Ltd.) and SiO_2 (99.0%, Hunan Huihong Reagent Co., Ltd.) to adjust the slag composition according to the required $w(FeO)/w(SiO_2)$ (weight ratio of FeO to SiO_2) and $w(CaO)/w(SiO_2)$ (weight ratio of CaO to SiO_2). FeO was used here for presentation convenience, although both Fe(III) and Fe(II) existed in the slag. Na_2CO_3 (99.9%, Sinopharm Chemical Reagent Co., Ltd.), coal powder (55.4 wt% carbon, 27.3 wt% volatiles and 16.8 wt% ash), and sulfur (99.0%, Hunan Huihong Reagent Co., Ltd.) were also added according to the set weight percent of the ES. The mixture was mixed in a mortar for 30 min before being transferred to a 500-mL fire clay crucible. After the furnace (SRJX-8-13, Changshi Furnace) temperature was raised to 650 °C, the crucible was transferred into the furnace, and the temperature was raised at 20 °C/min to 1250 °C. After smelting for 2 h, the crucible was lifted out of the furnace and cooled in the air atmosphere. Then, the crucible was broken, and the products, namely, matte and slag, were separated and weighed. Due to the low volatilities of Cu, Ni, and Cr compounds, their distribution in the flue dust during reduction was neglectable [17], thus, dust was not considered as a smelting product in this work. Finally, the Cu, Ni, and Cr contents in the products were analyzed.

The distribution ratio was calculated by Eqs. (2)–(3)

$$D_{\mathrm{MeM}} = \frac{m_{\mathrm{MeM}} \times \mathrm{M}_m}{M_{\mathrm{Me}}} \times 100\%, \tag{2}$$

$$D_{\mathrm{MeSl}} = \frac{m_{\mathrm{ESl}} \times M_{\mathrm{Sl}}}{M_{\mathrm{Me}}} \times 100\%, \tag{3}$$

where D_{MeM} and D_{ESl} denote the mass distribution ratios of metals (Me) in the matte and slag, m_{MeM} and m_{ESl} denote the weight ratios of metals in the matte and slag, M_{m} and M_{Sl} denote the weights of matte and slag produced in the smelting process, and M_{Me} denotes the total mass of metal (Me) in the ES.

Characterization

Composition Analysis

X-ray fluorescence spectrometer (XRF, XRF-1800, Shimadzu, Japan) was used to quantify element contents in the solid samples. The sample was scanned with a scanning rate of 20°/min by a tube current of 140 mA with an Rh target.

Inductively coupled plasma-atomic emission spectra (ICP-AES, ICAP 7400 Radial, Thermo Fisher Scientific, USA) were used to quantify the Cu, Ni, and Cr contents in the samples. When the standard solution with a concentration of 1 ppm or 10 ppm was measured, the RSD of ten consecutive measurements was less than 1.0%. First, standard curves were built based on Cu, Ni, and Cr standard solutions with various contents (National Nonferrous Metals and Electronic Materials Analysis and Testing Center, China). Second, the solid products, i.e., matte and slag, were digested in sulfuric (AR, Sinopharm Chemical Reagent Co., Ltd.) and phosphoric acid (AR, Sinopharm Chemical Reagent Co., Ltd.) mixtures, and then, the metal contents in the acid mixtures were analyzed.

Phase Analysis

X-ray diffraction pattern (XRD, Empyrean 2, PANalytical, Netherlands) was used to analyze the crystal phases of the samples with Cu Kα radiation ($\lambda = 1.5406$ Å). 2θ Ranging from 10° to 80° was scanned with a scanning rate of 10°/min, and the spectra were analyzed by Jade 6 using standard PDF cards (JCPDF cards) to obtain phase information.

Emission scanning electron microscopy (SEM, JSM-7900F, JEOL, Japan) was used to observe the morphology of the smelting products. The SEM was equipped with an energy-dispersive spectrometer (EDS, EDX-GENESIS60S, EDAX, USA) to analyze the micro-areas observed by SEM, and the working distance was 12 mm. The EDS data obtained in this study can be regarded as semi-quantitative only, with an uncertainty > ± 1 wt%. The samples were mounted with epoxy resin and polished. After preliminary

examination by optical microscopy, the samples were sputtered with carbon to improve the conductivity under an electron beam.

Toxicity Evaluation

The toxicities of the samples were evaluated by a standard toxicity characteristic leaching procedure (TCLP) according to the Chinese National Identification standards for hazardous wastes (GB5085.3-2007), as described in the Supplementary File.

Results and Discussion

Thermodynamic Analysis and Preliminary Investigation

Superimposed predominance diagrams of Cu–S–O, Ni–S–O and Cr–S–O at 1250 °C were depicted using the Predom module in FactSage 8.0 software [31], and the results are shown in Fig. 1. It suggests that Cu_2O and NiO in the ES can be reduced to Cu(l) and Ni(s) (Area (2)) at $\log P_{O_2} < -8$ atm, while Cr_2O_3 remains unchanged. In this regard, Cu and Ni will report to metal and Cr reports to slag in reductive smelting, which would realize their separation. However, due to its high melting point (1453 °C), Ni is in solid-state at 1250 °C, which accounts for the high smelting temperature for ES with high Ni contents [19]. On the other hand, Cu_2O and NiO can be converted to Cu_2S (l) and Ni_3S_2 (l) (Area (15)) by raising $\log P_{SO_2}$ at $\log P_{O_2} < -8$ atm, which would facilitate the enrichment of Ni and Cu in liquid matte at 1250 °C. Meanwhile, Cr remains to be solid Cr_2O_3. Therefore, the predominance diagram suggested that a matte smelting route would facilitate the enrichment of Ni and Cu and the separation of Cr at a typical matte smelting temperature.

According to the thermodynamic analysis, the ES was mixed with reduction and sulfurization agents, i.e., coal and sulfur powder, and preliminary matte smelting experiments were investigated with or without alkaline flux (Na_2CO_3). The conditions were $w(FeO)/w(SiO_2) = 1.5$, $w(CaO)/w(SiO_2) = 0.8$, the dosage of coal powder and sulfur powder = 10 wt% of the ES, the dosage of Na_2CO_3 = 38.2 wt% of the ES, smelting temperature = 1250 °C, and smelting time = 2 h. As shown in Fig. 2, neither homogeneous phases nor clear boundaries between different phases were identified in the sample without Na_2CO_3. The upper layer was dark gray glassy slag with white solid particles embedded, while the lower layer was heterogeneous mixed phases of slag and gray silver matte. Pores were also observed on this layer. The sample indicated that homogeneous molten phases were not produced without Na_2CO_3, leading to difficulties in not only matte making but also products separation. On the other hand, a clear boundary between the matte and slag can be observed in the sample with the addition of Na_2CO_3. The formation of homogeneous light–dark glassy slag and gray silver matte indicated that metal values were effectively enriched in the matte phase that can be separated from the

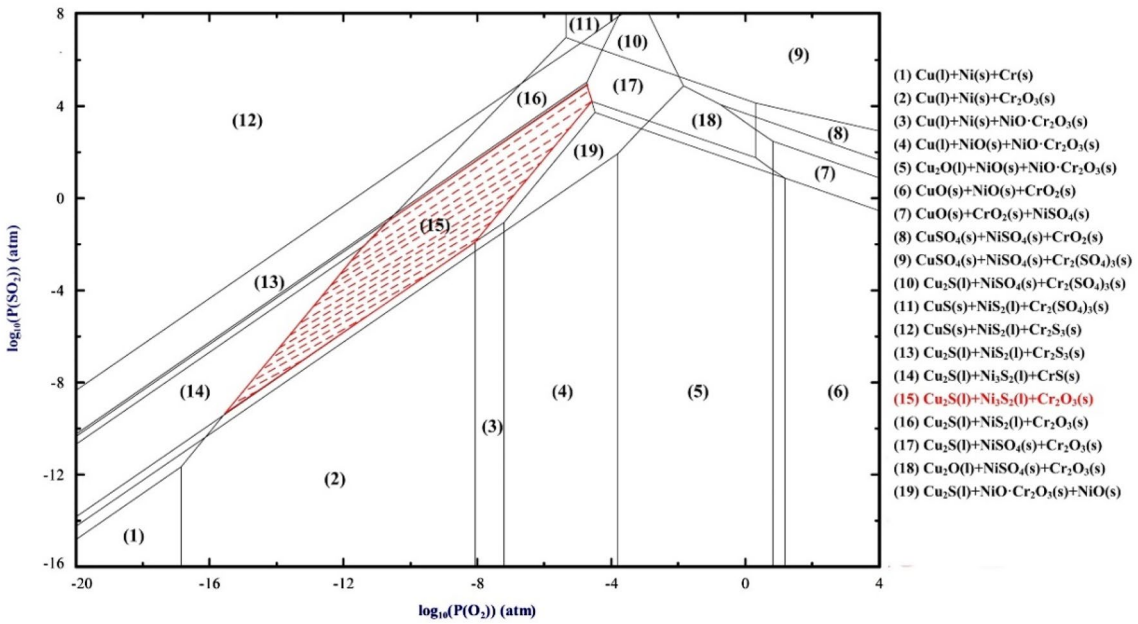

Fig. 1 Superimposed Cu–Ni–Cr–S–O predominance diagram at 1250 °C

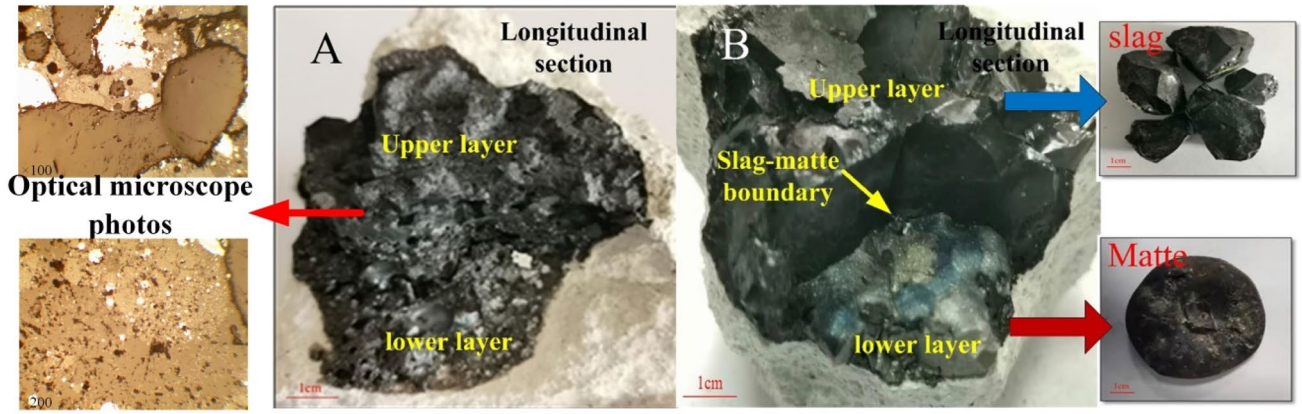

Fig. 2 Pictures of preliminary smelting products. Without Na_2CO_3 (**A**), and with Na_2CO_3 (**B**)

slag phase, suggesting that alkaline matte smelting was feasible to recover Cu and Ni in the ES at 1250 °C.

Effect of Na_2CO_3 Dosage

The effect of Na_2CO_3 dosage on the metal content of the smelting products was investigated under the following conditions: $w(FeO)/w(SiO_2) = 1.5$ and $w(CaO)/w(SiO_2) = 0.8$. The dosages of coal powder and sulfur powder were 4% and 8% of the ES weight, respectively. The smelting temperature and time of all the experiments were set at 1250 °C and 2 h otherwise mentioned.

As shown in Fig. 3A, B, the Cu and Ni contents of the slag decreased with increasing Na_2CO_3 dosage, while those of the matte increased. At a Na_2CO_3 dosage of 38.2%, the contents of Cu, Ni, and Cr of the slag (denoted as m_{CuSl}, m_{NiSl} and m_{CrSl}) were 0.2 wt%, 0.7 wt%, and 4.2 wt%, respectively, while those of the matte (denoted as m_{CuM}, m_{NiM} and m_{CrM}) were 19.0 wt%, 27.9 wt%, and 0.1 wt%, respectively. In accordance with the content, the matte distribution ratio of Cu and Ni (denoted as D_{CuM} and D_{NiM}) reached 95.1% and 90.1%, and that of Cr in the slag (denoted as D_{CrSl}) amounted to 99.3%, as shown in Fig. 3C. This result indicated that the increase of Na_2CO_3 dosage was conducive to recovering Cu and Ni but had little effect on Cr distribution. Although a further increase in Na_2CO_3 dosage may lead to even higher recovery ratios, considering that m_{CuSl} and m_{NiSl} were already below 1 wt% at a Na_2CO_3 dosage of 38.2%, great improvement in metal recovery was not expected by a further increase of Na_2CO_3 dosage.

Effect of Coal Dosage

Coal powder was used as an agent to produce a reductive atmosphere. The effect of coal powder was investigated by varying the coal dosage from 2 to 13% of the ES weight, and fixing other conditions: $w(FeO)/w(SiO_2) = 1.5$ and $w(CaO)/w(SiO_2) = 0.8$, and the dosages of Na_2CO_3 and sulfur powder were 38.2% and 10% of the ES weight.

According to Fig. 4A, m_{CuSl}, m_{NiSl}, and m_{CrSl} all increased with increasing coal dosage. With a coal dosage of 2%, m_{CuSl}, m_{NiSl}, and m_{CrSl} were 0.2 wt%, 0.4 wt%, and 2.2 wt%, which rose to 1.5 wt%, 1.0 wt%, and 5.7 wt%, respectively, with a coal dosage of 13%. Meanwhile, m_{CuM}, m_{NiM}, and m_{CrM} decreased by 3.8 wt%, 1.3 wt%, and 1.7 wt%, respectively (Fig. 4B). Figure 4C shows the effect of coal dosage on the element distribution. This result indicated that Cu and Ni were mainly reported to the matte, while Cr was reported to the slag. D_{CuM}, D_{NiM}, and D_{CrM} were 94.9%, 92.3%, and 4.8%, respectively, with a coal dosage of 2 wt%. Increasing the coal dosage to 4 wt% resulted in a decrease of D_{CrM} to 1.3%, while D_{CuM} and D_{NiM} remained almost unchanged. A further increase in coal dosage led to decreases of D_{CuM} and D_{NiM}; in particular, D_{CuM} sharply decreased to 77.5% with a 13% coal dosage. Although coal powder was necessary for reducing metal oxides, its negative effect on metal recovery at high coal dosages could be attributed to two reasons: first, a strong reductive atmosphere may lead to the formation of metal; second, a higher coal dosage may lead to more ash containing refractory oxides, as proved by composition analysis (Table 2), the content of aluminum oxides raised with the increase of coal dosage, which may raise the viscosity and melting point of the slag. Therefore, a 4% coal dosage was chosen to be the optimal condition.

Effect of Sulfur Dosage

The effect of sulfur dosage was studied by changing from 4 to 12% of the ES weight, while fixing other conditions as $w(FeO)/w(SiO_2) = 1.5$ and $w(CaO)/w(SiO_2) = 0.8$, and the dosages of Na_2CO_3 and coal powder were 38.2% and 4% of the ES weight.

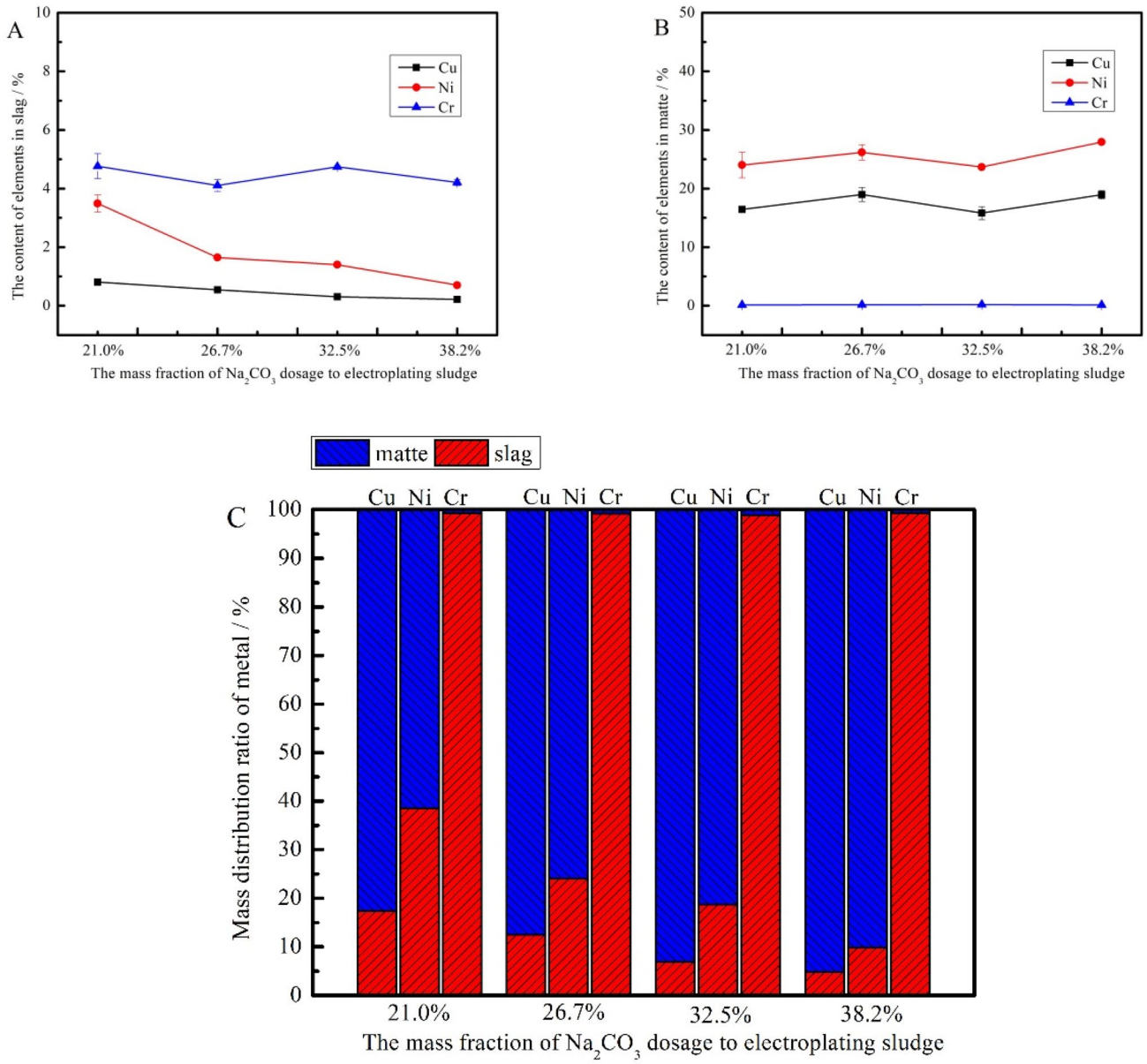

Fig. 3 Effect of the mass fraction of Na_2CO_3 dosage to electroplating sludge on the metal content in the slag (**A**), matte (**B**) and on the mass distribution ratio of metal (**C**)

As shown in Fig. 5A, B, m_{CuSl}, m_{NiSl}, and m_{CrSl} decreased from 0.4 wt%, 1.4 wt%, and 4.7 wt% to 0.3 wt%, 0.7 wt%, and 3.4 wt% by raising the sulfur dosage from 4 to 10%. This can be explained by the fact that a higher sulfur dosage facilitated the formation of Cu_2S and Ni_3S_2, which reduced their content in the slag. Meanwhile, the Fe content of the matte (denoted as m_{FeM}) also increased, as implied by the drop of m_{CuM} and m_{NiM}. Consistently, Sridhar et al. [32] studied Cu loss in smelting slag and pointed out that m_{CuSl} decreased with increasing m_{FeM}. However, a further increase in sulfur dosage to 12 wt% led to higher m_{CuSl}, m_{NiSl}, and m_{CrSl}, which could be attributed to the movement of slag composition to the CaO–SiO_2 side with excessive Fe reported to the matte phase, as the increase in $[SiO_4]^{4-}$ content would raise the viscosity of the slag, leading to bad separation of the smelting products. Figure 5C shows the element distributions at various sulfur dosages. This result suggested that D_{CuM} and D_{NiM} increased with increasing sulfur dosage before 10%; however, sulfur dosages higher than 8% showed little effect on improving Cu recovery; therefore, an 8% sulfur dosage would be optimal for Cu and Ni recovery.

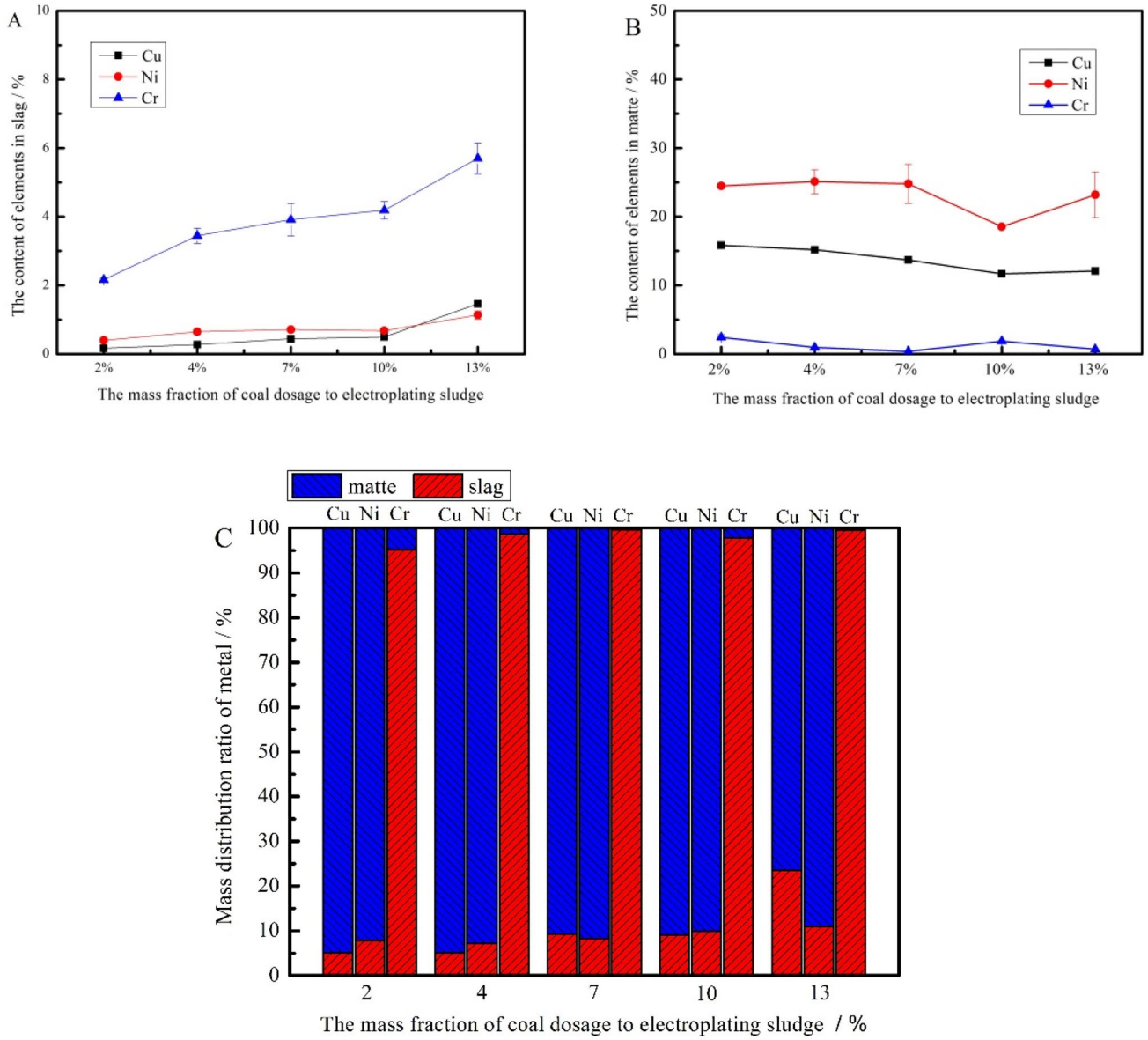

Fig. 4 Effect of the mass fraction of coal dosage to electroplating sludge on the metal content in the slag (**A**), matte (**B**) and on the mass distribution ratio of metal (**C**)

Effect of $w(FeO)/w(SiO_2)$

The effect of $w(FeO)/w(SiO_2)$ ranging from 1.1 to 1.9 was studied using the conditions of $w(CaO)/w(SiO_2) = 0.8$, and the dosages of Na_2CO_3, coal powder, and sulfur were 38.2%, 4%, and 8% of the ES weight, respectively.

Figure 6A, B indicates that m_{CuSl} and m_{NiSl} decreased before $w(FeO)/w(SiO_2) = 1.5$ and then slightly increased, while m_{CrSl} showed a downward trend. The possible reason for this could be that the increase of $w(FeO)/w(SiO_2)$ within a certain range is beneficial for the sedimentation of metal droplets [33], but excessive FeO_x resulted in the movement of slag composition toward the FeO_x apex, where the formation of solid spinel with high melting points is favored at a prevailing partial pressure of matte smelting, i.e., approximately 10^{-8} atm. Figure 6C suggests a consistent trend in which the optimal Cu and Ni recoveries were achieved at $w(FeO)/w(SiO_2) = 1.5$, D_{CuM} and D_{NiM} were 95.1% and 90.1%, respectively, while D_{CrSl} reached 99.3%.

Effect of $w(CaO)/w(SiO_2)$

The effect of $w(CaO)/w(SiO_2)$ ranging from 0.6 to 0.9 was studied using the conditions of $w(FeO)/w(SiO_2) = 1.5$, and the dosages of Na_2CO_3, coal powder, and sulfur were 38.2%, 4%, and 8% of the ES weight, respectively.

Table 2 Main composition of the smelted products of several experiments (wt%)

Exp. nos	Product	Fe	Cu*	Ni*	Cr*	Zn	Na	Ca	Al	Mg	Si	S
E1	Matte	16.3	19.0	27.8	0.1	1.0	4.8	0.6	2.0	0.1	2.6	20.4
	Slag	14.6	0.2	0.7	4.2	2.6	11.8	7.5	7.6	0.5	15.3	5.3
E2	Matte	14.2	16.5	24.0	0.2	0.8	4.1	0.6	0.9	0.1	1.5	16.3
	Slag	16.3	0.8	3.5	4.8	2.9	10.1	7.8	8.6	0.6	16.2	0.7
E3	Matte	22.3	15.2	23.4	1.0	2.2	4.3	0.2	0.3	0.1	0.3	24.1
	Slag	12.6	0.3	0.7	3.4	3.1	10.8	11.8	7.8	0.9	16.4	1.24
E4	Matte	22.9	12.1	23.2	0.7	3.0	6.5	0.2	0.2	0.1	0.2	26.7
	Slag	9.4	1.5	1.1	5.7	2.1	12.2	11.5	9.4	0.8	18.6	1.2
E5	Matte	2.4	22.3	30.6	0.3	0.4	4.5	1.1	2.9	0.1	4.2	13.7
	Slag	17.3	0.4	1.4	4.7	2.7	14.1	7.7	7.8	0.5	15.5	1.1
E6	Matte	15.7	14.2	19.3	0.05	1.8	8.4	0.6	1.7	0.1	2.2	19.5
	Slag	13.1	0.9	2.2	4.4	2.6	13.1	7.8	9.5	0.6	16.7	1.0

*Analyzed by ICP-AES

According to Fig. 7A, B, the effect of $w(CaO)/w(SiO_2)$ was similar to that of $w(FeO)/w(SiO_2)$. The optimal $w(CaO)/w(SiO_2)$ was found to be 0.8, by which the lowest m_{CuSl} and m_{NiSl} were obtained. Consistently, Fig. 7C suggests that D_{CuM}, D_{NiM}, and D_{CrSl} were the highest in this condition. Nikolic et al. [34] and Shishin et al. [35] suggested that an increase in CaO content in the FeO_x–SiO_2–CaO slag system raised the activity coefficient of Cu in the slag, which was conducive to reducing its distribution in the slag.

Composition and Phase Analysis of the Smelting Products

The composition of some smelting products is analyzed by XRF and is listed in Table 2, and the conditions of obtaining these products are listed in Table S1. It can be informed that the Cu + Ni content of the matte ranged from 33.5 to 52.9 wt%, as described in the previous sections. It is noted that $w(FeO)/w(SiO_2)$ and $w(CaO)/w(SiO_2)$ in the slag were lower than the set values, which can be ascribed to the deportment of Fe to the matte phase and the reaction between the slag and crucible.

SEM–EDS and XRD analyses were performed to obtain phase information of the smelting products, namely, matte and slag, as shown in Figs. 8 and 9. As shown in Fig. 8A, there were two distinguishable contrasts in the slag. EDS mapping figures revealed that Fe and Cr were concentrated in the brighter area, Na distributed evenly, while Cu and Ni were almost negligible in the whole sample. Based on the EDS analysis of the respective points (Table 3), the brighter phase was mainly spinel phases of $FeCr_2O_4$, $NiCr_2O_4$, $FeAl_2O_4$, Fe_3O_4, or their composites, which is consistent with the XRD analysis (Fig. 9). The darker one was the glassy slag.

It is also worth mentioning that Cr was mainly detected in the spinel phases rather than the glassy slag phase. According to the phase diagram of the slag at 1250 °C (Fig. S3), liquid slag equilibrated with spinel during smelting. As the sample was not quenched but cooled in air after the experiment, the occurrence of Cr-containing spinel can be either a solid phase at the smelting temperature or formed during the cooling. The glassy slag had a higher Na content than the other phases, which could account for the lower smelting temperature of the alkaline smelting technique. On the other hand, SEM–EDS analysis of the matte revealed the existence of $Cu_{2-x}FeS$ and $Ni_{3-x}Fe_xS_2$, in accordance with the XRD results. EDS mapping revealed that the distribution of Na was highly coincident with that of Cu, suggesting that Na_2S indeed combined with Cu_2S during the matte making. In fact, EDS analysis for point 4 (Table 3) also revealed a Na content of 9.4 wt% in the $Cu_{2-x}Fe_xS$ matte, which is in accordance with the EDS mapping analysis.

Discussion

The liquidus temperature of slag is a determining factor in regard to the smelting temperature. According to the FeO_x–CaO–SiO_2 ternary [29], the liquidus is approximately 1200–1250 °C at $w(FeO)/w(SiO_2) = 1.5$, $w(CaO)/w(SiO_2) = 0.8$ and $\log P_{O_2} = -8$ atm. In this regard, the ES can theoretically be smelted at 1250 °C. However, the presence of Cr in the ES hindered the smelting process due to its effect on raising the liquidus temperature. Sukhomlinov et al. [36] pointed out that the solubility of Cr in a FeO_x–SiO_2–CaO (0–10 wt%) system was only 0.3 wt% in a reducing condition (PO_2=10^{-10} atm). Excessive Cr over the solubility in the slag system promoted the formation of a high melting point spinel phase, which led to an increase in the liquidus temperature by 50–60 °C, as reported by Ilyushechkin et al. [37].

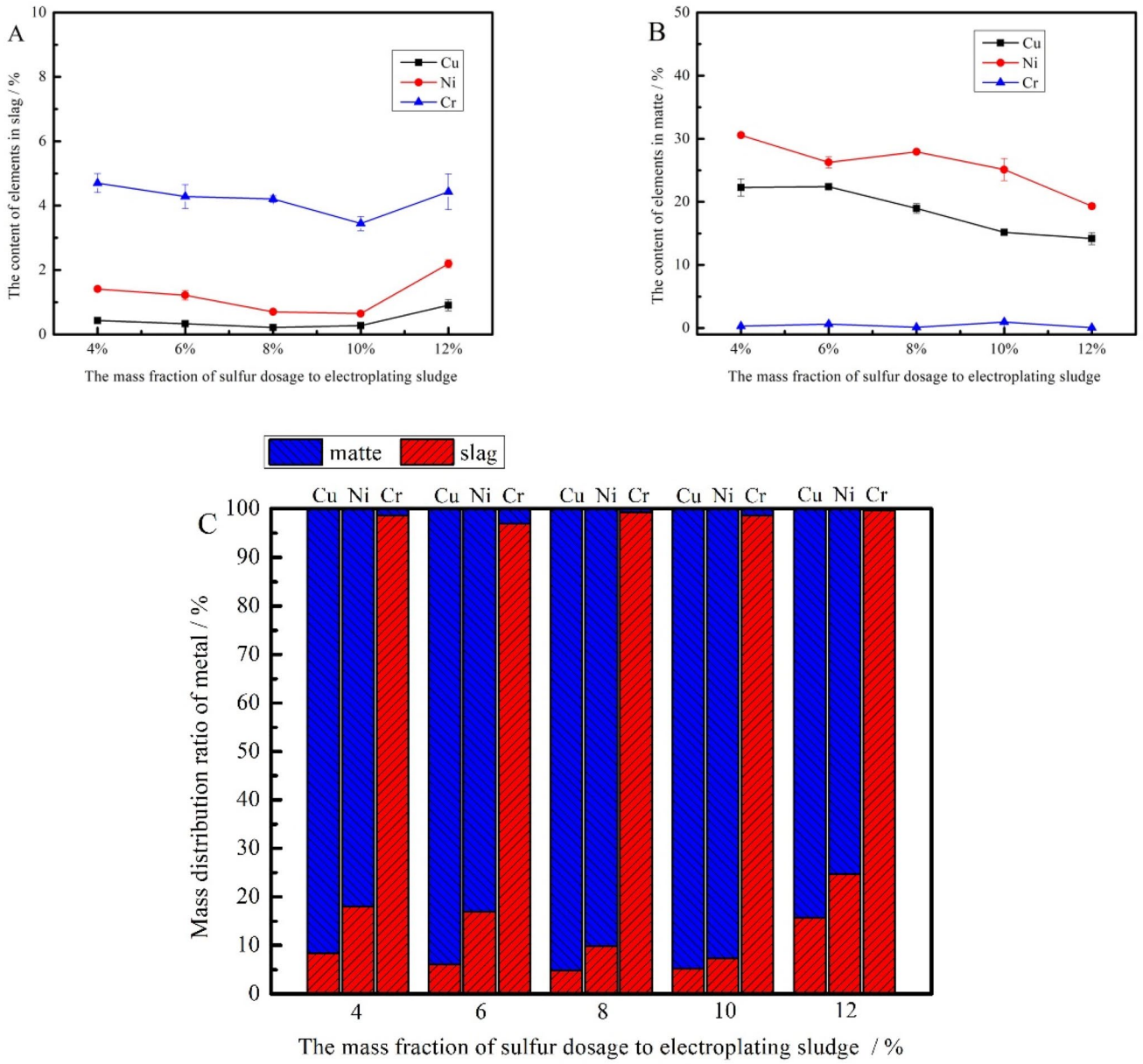

Fig. 5 Effect of the mass fraction of sulfur dosage to electroplating sludge on the metal content in the slag (**A**), matte (**B**) and on the mass distribution ratio of metal (**C**)

The addition of alkaline flux, i.e., Na_2CO_3, facilitated the smelting of ES at a typical nonferrous metal smelting temperature (1250 °C), which is 100–250 °C lower than those reported in previous works [17, 19]. As shown in Fig. 2, slag and matte were distinguishably separated compared with the products without Na_2CO_3 addition. Figure 8 further shows that Cu and Ni sulfides were enriched in the matte phase, while Cr was deported to the slag phase. This could be attributed to two reasons:

Firstly, the introduction of alkaline flux reduced the melting temperature of the slag. FactSage 8.0 was used to simulate the effect of Na_2O addition on the isotherms of pseudo FeO–SiO_2–CaO with 5.8 wt% Cr_2O_3 (equals to 4 wt% Cr) at 1250 °C and $\log P_{O_2} = -8$ atm. The boundary conditions for the calculation are listed in the Supplementary File. Although the system was simplified for calculation convenience and may not reflect the real melting point of the experimental slag system, the liquidus at the set slag composition [red dots in Fig. 10 (color figure online)] was reduced by over 40 °C with the addition of 13.5% Na_2O (equal to 10 wt% Na). The main reason for the extremely high liquidus of the slag was due to the high temperature required to fully melt chromium compounds, e.g., $FeCr_2O_4$, etc. However, the

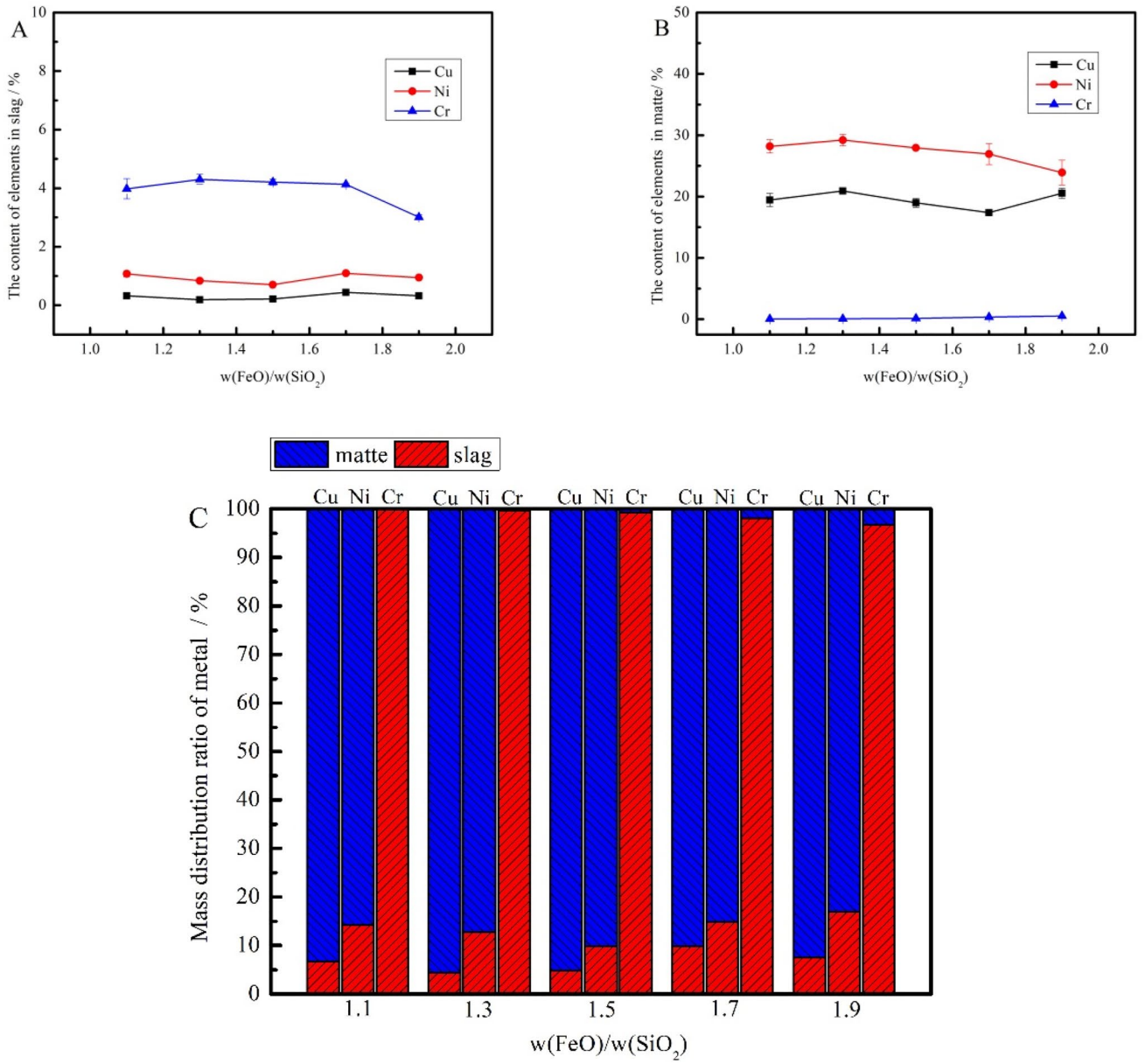

Fig. 6 Effect of $w(FeO)/w(SiO_2)$ on the metal content in the slag (**A**), matte (**B**) and on the mass distribution ratio of metal (**C**)

proportion of these solid compounds in the liquid slag may be influenced by alkaline flux.

As shown in Fig. 11, the effect of Na_2O on the proportion of equilibrium phases, i.e., liquid slag and solid spinel, of the product was calculated at 1250 °C and $\log P_{O_2} = -8$ atm (Fig. 11; Table S2). The results indicated that solid spinel proportion decreased from 31.5 to 10.9% as $Na_2O/(FeO + SiO_2 + CaO + Cr_2O_3)$ increased from 0 to 15 wt%, which was the main reason why alkaline smelting of ES can be conducted at a lower temperature.

Secondly, although Mäkinen and Taskinen [38] reported the liquidus of copper–nickel mattes could be below 600 °C, the addition of Na_2CO_3 led to the formation of Na_2S, which could further reduce the melting point of Cu–Ni–Fe sulfides, as has been reported in copper dross smelting processes [27, 39].

The element distribution results indicated that 95.1% Cu and 90.1% Ni of the ES were recovered in the matte after the alkaline smelting process. Although the data cannot be directly compared with other studies due to the different raw materials and final products, Cu and Ni recovery were close to those of the carbon thermal reduction–reduction refining process (Cu recovery: 96.4%, Ni recovery: 85%) for ES with a high Cu content (24 wt%) and low Cr content (0.47 wt%) [17], suggesting that the alkaline smelting technique can effectively recover Cu and Ni in the ES with 10 times

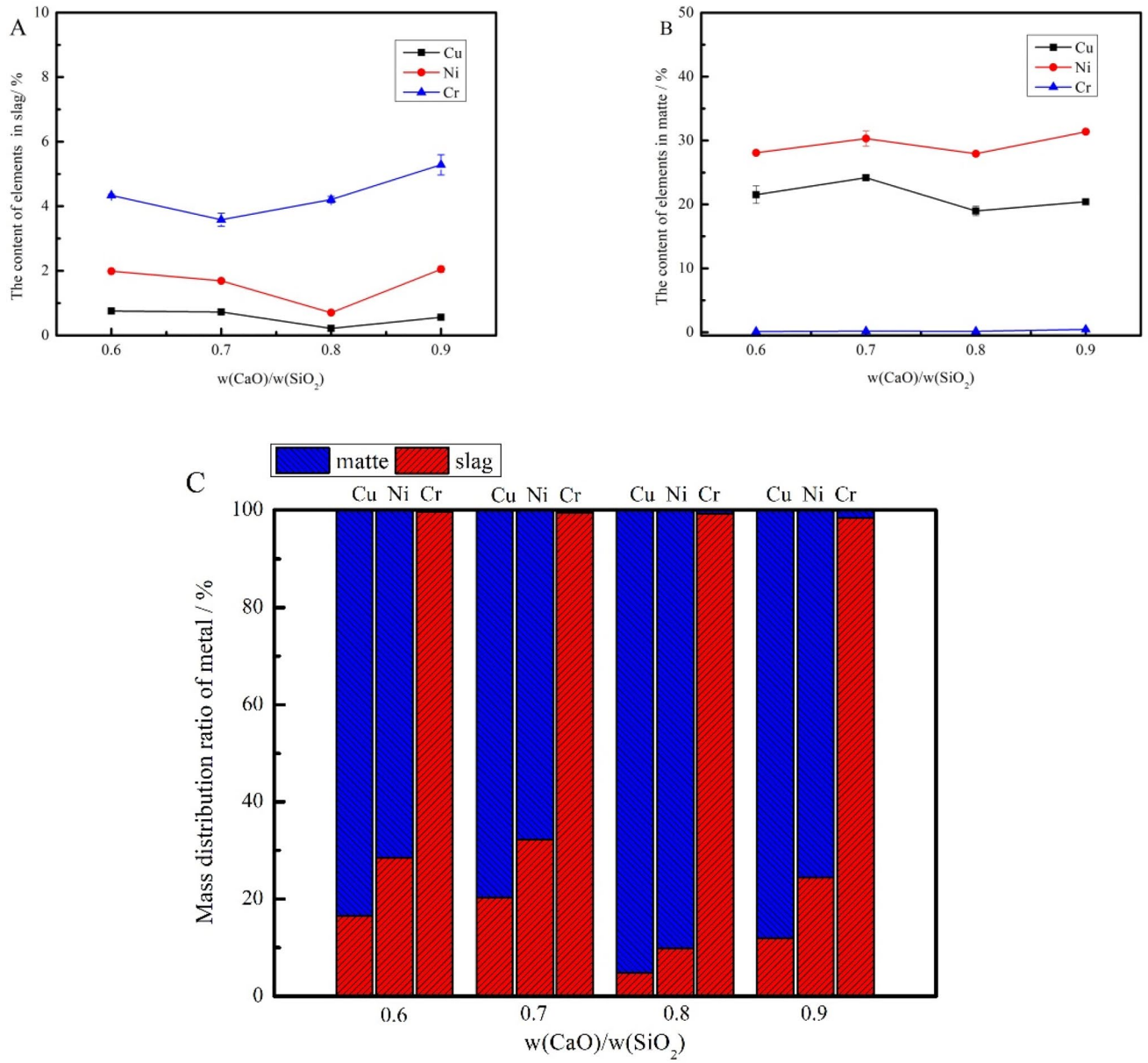

Fig. 7 Effect of $w(CaO)/w(SiO_2)$ on the metal content in the slag (**A**), matte (**B**) and on the mass distribution ratio of metal (**C**)

higher Cr content using a relatively lower smelting temperature, i.e., 1250 °C.

The cost–benefit analysis is listed in Table 4. To simplify the calculation, the labor cost of the operation certainly depends on the scale of the operation was omitted. In addition, the prices of the raw material used in the calculations retrieved from a raw material wholesale sales platform operated by Alibaba Group (https://www.1688.com). The reagent and electricity cost of the present technique for the ES would be approximately 1600 RMB/t_{ES}, which is far below the landfill charge for hazardous solid waste (2700 RMB/t) [40]. Moreover, the recovered Cu and Ni can also be profitable products. In this regard, the alkaline smelting technique for ES is economically feasible.

On the other hand, over 99% Cr was reported to the slag after the alkaline smelting process. Typically, Cr was extracted from chromium ores by a soda roasting process in which Cr_2O_3 was transferred into soluble Na_2CrO_4 for a higher leaching ratio. In this regard, alkaline smelting slag may also pollute the environment by releasing soluble Cr, Cu, Ni, or other heavy metals. To test its toxicity, the TCLP process [42] was applied to the slag produced in the optimal smelting condition, and the results are listed in Table 5. The concentrations of Cu, Ni, Cr, Pb, and Zn in the leachate were 0.17 mg/L, 0.15 mg/L, 0.25 mg/L,

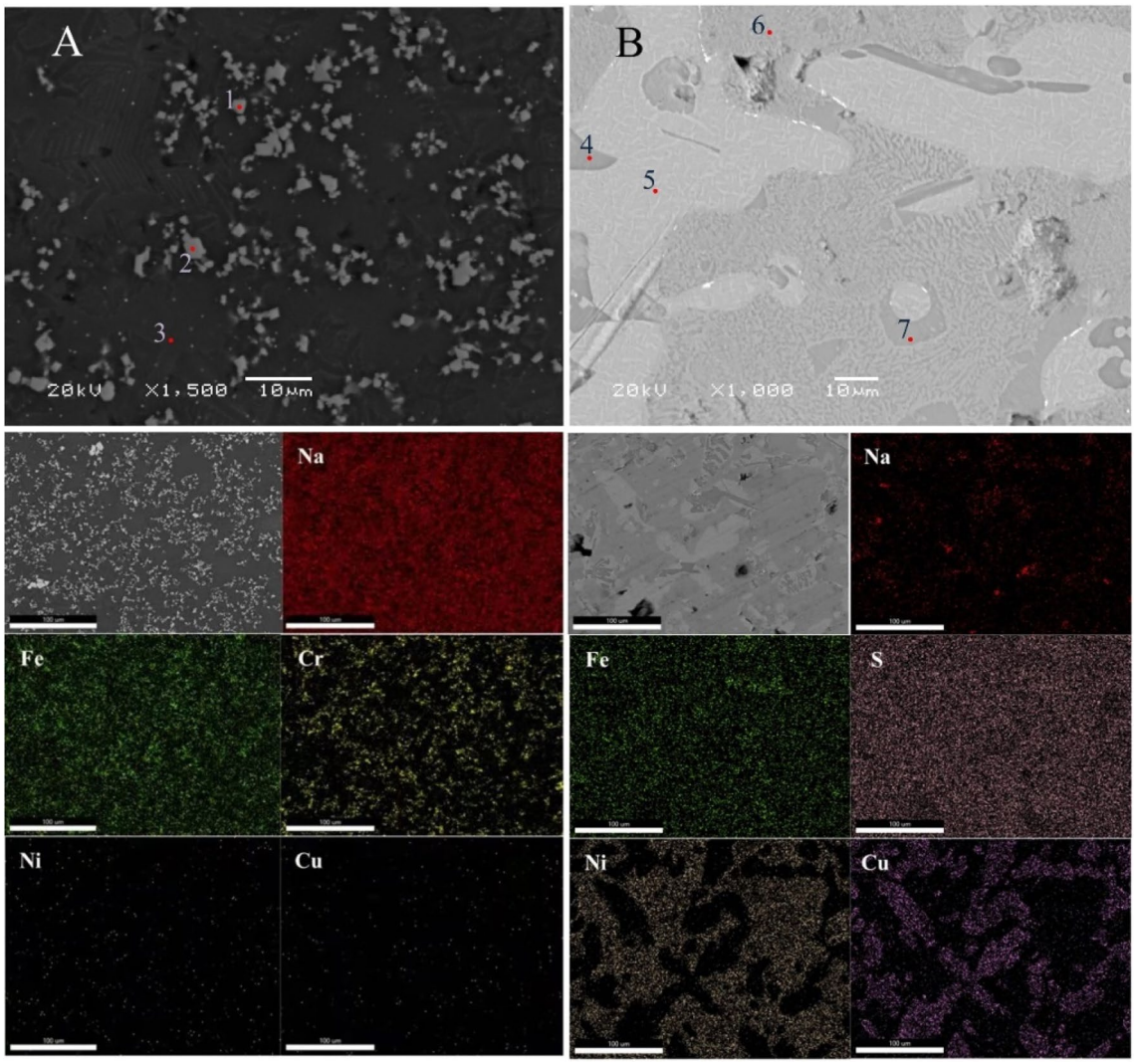

Fig. 8 SEM–EDS figures of the smelting products (**A** slag, **B** matte)

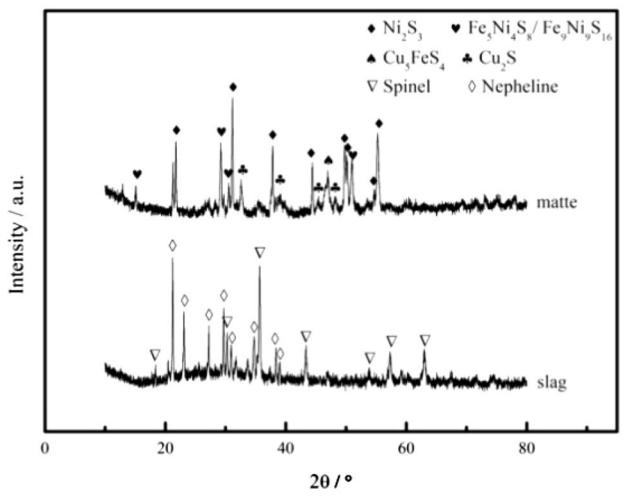

Fig. 9 XRD patterns of the smelting products

0.06 mg/L, and 0.17 mg/L, respectively, which are below the standard of extraction toxicity of hazardous waste in China [42] and in the US [43, 44]. As indicated by SEM–EDS analysis (Fig. 8), Cr, Cu, Ni, and Zn mainly existed in the form of (Fe, Ni, Cu, Zn)Cr_2O_4 spinel which was reported to be a stable phase resistant to leaching [6]. Moreover, the diffusion of leaching solution to the spinel phases was further prohibited by the encapsulation of spinel in the glassy slag matrix [45].

Conclusions

Alkaline matte smelting was proposed for recovering Cu and Ni in the ES, and the effect of various smelting parameters on the distribution of metal values was investigated in this work. The main conclusions are as follows:

Table 3 EDS analysis results of the points in Fig. 8

Points	Content (wt%)											Main phase
	Fe	Si	Ca	Cr	Ni	Cu	Zn	Al	Na	S	O	
1	15.1	5.1	1.7	20.8	1.6	–	3.6	5.4	5.8	–	37.2	Spinel
2	19.7	1.5	0.9	34.2	2.3	0.7	–	–	6.0	–	34.8	Spinel
3	4.6	16.9	6.0	–	–	–	0.8	9.6	15.3	–	44.4	Slag
4	12.8	–	–	–	–	43.9	–	–	9.4	27.9	0.8	$Cu_{2-x}Fe_xS$
5	7.7	–	–	–	–	65.9	–	–	–	26.4	–	$Cu_{2-x}Fe_xS$
6	9.4	–	–	–	47.3	3.6	–	–	–	26.5	1.9	$Ni_{3-x}Fe_xS_2$
7	26.0	–	–	–	32.4	1.6	–	–	–	32.5	–	$Ni_{3-x}Fe_xS_2$

"–" Not detected or not exist

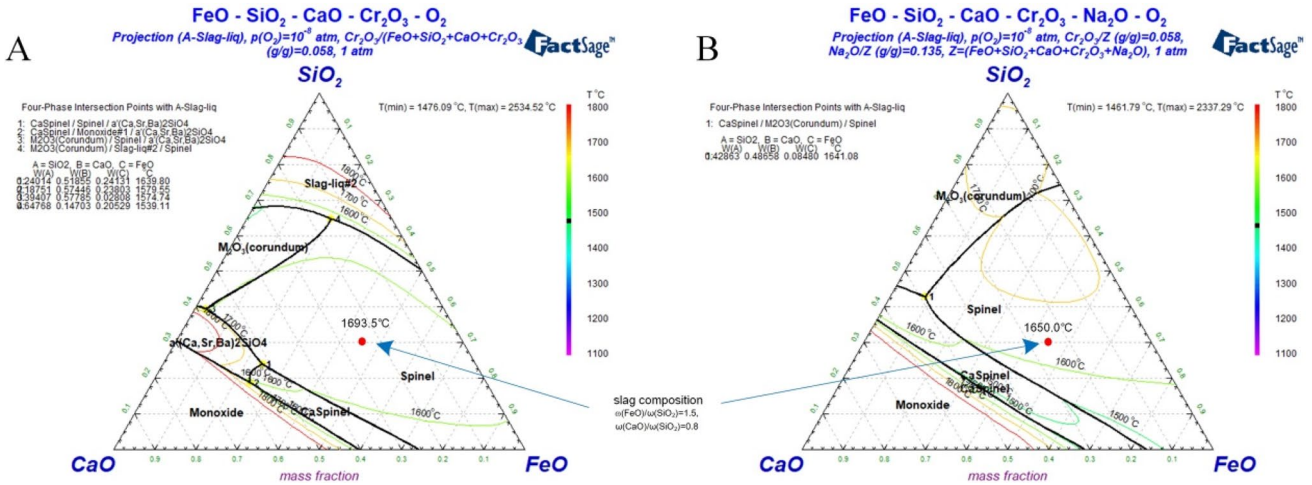

Fig. 10 The effect of Na_2O on isotherms of FeO–CaO–SiO_2 pseudo-ternary. **A** Without Na_2O, and **B** with 13.5% Na_2O

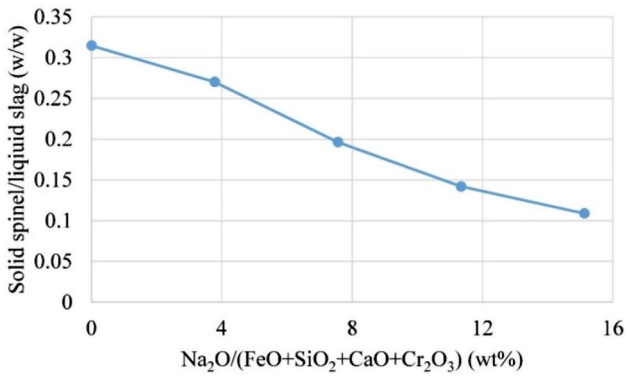

Fig. 11 Effect of Na_2O on the mass ratio of solid spinel to liquid slag

Table 4 Cost–benefit analysis of the alkaline smelting technique for ES

	Price (RMB/t)	Consumption (t/t_{ES})	Cost (RMB)
Soda	1050	0.38	399
Coal	800	0.04	30
Sulfurization agent	2000	0.08	160
lime	480	0.13	62.2
Electricity*	0.73 RMB/kW·h	650 kW·h/t × 2 h	949
Total cost			1600.2

*Calculation based on the average industrial electricity price and power consumption of smelting Cu–Ni ore calcines in an electrical furnace [41]

(1) The alkaline matte smelting technique effectively enriched Cu and Ni in the matte phase and Cr oxide in the slag phase. Matte and slag were well separated with a clear boundary at a typical nonferrous metal smelting temperature, i.e., 1250 °C, which is 100–250 °C lower than the temperatures previously reported. Cost benefit analysis indicated that the processing cost for the ES was 1600.2 RMB/t, showing a high potential for industrial application.

(2) The optimal process condition was obtained as $w(FeO)/w(SiO_2) = 1.5$, $w(CaO)/w(SiO_2) = 0.8$, Na_2CO_3, coal powder, and sulfur dosages were 38.2%, 4%, and

Table 5 Leaching toxicity of the alkaline smelting slag (mg/L)

Sample	Cu	Ni	Cr	Pb	Zn
Slag	0.17	0.15	0.25	0.06	0.17
Standard*	100	5	15	5	100
Standard**	–	–	5.0	5.0	–

*GB5085.3-2007

**Code of Federal Regulations (2022) 261.24 Toxicity characteristic

– Not mentioned in the US Federal Regulations ((2022) 261.24)

8% of the ES weight, in which D_{CuM}, D_{NiM}, and D_{CrSl} reached 95.1%, 90.1%, and 99.3%, respectively.

(3) The TCLP test indicated that the Cu, Ni, Cr, Pb, and Zn leaching toxicities of the slag were much lower than the Chinese national identification standards for hazardous wastes (GB5085.3-2007) and the US Federal Regulations ((2022) 261.24). The formation of stable spinel phases containing Cu, Ni, Cr, and Zn, plus their embedment in the glassy slag matrix, could be accounted for the low toxicity.

Supplementary Information The online version of this article (https://doi.org/10.1007/s40831-022-00545-5) contains supplementary material, which is available to authorized users.

Acknowledgements The financial supports by National Key Research and Development Program of China (2018YFC1901604) and Natural Science Foundation of Hunan Province (No. 2018JJ3662) are gratefully acknowledged. The valuable comments by the reviewers are gratefully acknowledged.

Declarations

Conflict of interest All authors declare that they have no conflict of interest.

References

1. Yan K, Liu Z, Li Z, Yue R, Guo F, Xu Z (2019) Selective separation of chromium from sulphuric acid leaching solutions of mixed electroplating sludge using phosphate precipitation. Hydrometallurgy 186:42–49. https://doi.org/10.1016/j.hydromet.2019.03.013
2. Zhang B, Wang Y, Tang X, Wang S, Wei C, Wang R, Zhang W (2019) Oxidation of high iron content electroplating sludge in supercritical water: stabilization of zinc and chromium. Environ Sci Pollut Res Int 26(15):15001–15010. https://doi.org/10.1007/s11356-019-04897-6
3. Chen H, Yuan H, Mao L, Hashmi MZ, Xu F, Tang X (2020) Stabilization/solidification of chromium-bearing electroplating sludge with alkali-activated slag binders. Chemosphere 240:124885. https://doi.org/10.1016/j.chemosphere.2019.124885
4. Hu S, Hu J, Sun Y, Zhu Q, Wu L, Liu B, Xiao K, Liang S, Yang J, Hou H (2021) Simultaneous heavy metal removal and sludge deep dewatering with Fe(II) assisted electrooxidation technology. J Hazard Mater 405:124072. https://doi.org/10.1016/j.jhazmat.2020.124072
5. Cai XW, Wei XG, Du CM (2020) Thermal plasma treatment and co-processing of sludge for utilization of energy and material. Energy Fuels 34(7):7775–7805. https://doi.org/10.1021/acs.energyfuels.0c00572
6. Mao L, Tang R, Wang Y, Guo Y, Su P, Zhang W (2018) Stabilization of electroplating sludge with iron sludge by thermal treatment via incorporating heavy metals into spinel phase. J Clean Prod 187:616–624. https://doi.org/10.1016/j.jclepro.2018.03.235
7. Zhang Y, Shi P, Chen L, Tang Q (2018) Utilization of electroplating sludge as subgrade backfill materials: mechanical and environmental risk evaluation. Adv Civ Eng 2018:4891418. https://doi.org/10.1155/2018/4891418
8. Dai Z, Zhou H, Zhang W, Hu L, Huang Q, Mao L (2019) The improvement in properties and environmental safety of fired clay bricks containing hazardous waste electroplating sludge: the role of Na_2SiO_3. J Clean Prod 228:1455–1463. https://doi.org/10.1016/j.jclepro.2019.04.274
9. Yue Y, Zhang J, Sun F, Wu S, Pan Y, Zhou J, Qian G (2019) Heavy metal leaching and distribution in glass products from the co-melting treatment of electroplating sludge and MSWI fly ash. J Environ Manag 232:226–235. https://doi.org/10.1016/j.jenvman.2018.11.053
10. Wu P, Zhang LJ, Liu YD, Xie XX, Zhou J, Jia HH, Wei P (2019) Enhancing Cu–Zn–Cr–Ni co-extraction from electroplating sludge in acid leaching process by optimizing Fe^{3+} addition and redox potential. Environ Eng Sci 36(9):1244–1257. https://doi.org/10.1089/ees.2019.0127
11. Zhang L, Zhou W, Liu Y, Jia H, Zhou J, Wei P, Zhou H (2020) Bioleaching of dewatered electroplating sludge for the extraction of base metals using an adapted microbial consortium: process optimization and kinetics. Hydrometallurgy 191:105227. https://doi.org/10.1016/j.hydromet.2019.105227
12. Huyen PT, Dang TD, Mai TT, Huyen N, Roy S (2016) Electrochemical copper recovery from galvanic sludge. Hydrometallurgy 164:295–303. https://doi.org/10.1016/j.hydromet.2016.06.028
13. Peng G, Deng S, Liu F, Li T, Yu G (2020) Superhigh adsorption of nickel from electroplating wastewater by raw and calcined electroplating sludge waste. J Clean Prod 246:118948. https://doi.org/10.1016/j.jclepro.2019.118948
14. Weng C, Sun X, Han B, Ye X, Zhong Z, Li W, Liu W, Deng H, Lin Z (2020) Targeted conversion of Ni in electroplating sludge to nickel ferrite nanomaterial with stable lithium storage performance. J Hazard Mater 393:122296. https://doi.org/10.1016/j.jhazmat.2020.122296
15. Ye X, Lin Z, Liang S, Huang X, Qiu X, Qiu Y, Liu X, Xie D, Deng H, Xiong X, Lin Z (2019) Upcycling of electroplating sludge into ultrafine Sn@C nanorods with highly stable lithium storage performance. Nano Lett 19(3):1860–1866. https://doi.org/10.1021/acs.nanolett.8b04944
16. Shen H, Liu B, Shi Z, Zhao S, Zhang J, Zhang S (2021) Reduction for heavy metals in pickling sludge with aluminum nitride in secondary aluminum dross by pyrometallurgy, followed by glass ceramics manufacture. J Hazard Mater 418:126331. https://doi.org/10.1016/j.jhazmat.2021.126331
17. Tian L, Chen L, Gong A, Wu X, Cao C, Liu D, Chen Z-Q, Xu Z-F, Liu Y (2020) Separation and extraction of valuable metals from electroplating sludge by carbothermal reduction and low-carbon reduction refining. JOM 72(2):782–789. https://doi.org/10.1007/s11837-019-03880-3
18. Zhou C, Ge S, Yu H, Zhang T, Cheng H, Sun Q, Xiao R (2018) Environmental risk assessment of pyrometallurgical residues derived from electroplating and pickling sludges. J Clean Prod 177:699–707. https://doi.org/10.1016/j.jclepro.2017.12.285

19. Zhou L, Yan X, Wu M, Li Y, Wang L, Zhu L, Bing N, Qiao Y, Wang L (2016) Research on reduction and recovery metals from electroplating sludge by potato starch. J Shanghai Polytech Univ 33(1):27–30. https://doi.org/10.19570/j.cnki.jsspu.2016.01.005
20. Zhang D, Reng G, Yang T, Liu W, Chen L, Liu R (2019) A harmless method for disposaling electroplating sludge. Chinese Patent 201911340666.0
21. Yue T, Niu Z, Hu Y, Han H, Lyu D, Sun W (2019) Cr(III) and Fe(II) recovery from the polymetallic leach solution of electroplating sludge by Cr(III)–Fe(III) coprecipitation on maghemite. Hydrometallurgy 184:132–139. https://doi.org/10.1016/j.hydromet.2018.11.013
22. Ma Y, Zhou X, Tang J, Liu X, Gan H, Yang J (2021) One-step selective recovery and cyclic utilization of valuable metals from spent lithium-ion batteries via low-temperature chlorination pyrolysis. Resour Conserv Recycl 175:105840. https://doi.org/10.1016/j.resconrec.2021.105840
23. Chen B, He J, Sun X, Zhao J, Jiang H, Zhang L (2020) Separating and recycling metal mixture of pyrolyzed waste printed circuit boards by a combined method. Waste Manag 107:113–120. https://doi.org/10.1016/j.wasman.2020.04.006
24. Guo X-Y, Liu J-X, Tian Q-H, Li D (2013) Principle and method of low temperature alkaline smelting in non-ferrous metallurgy complicated resources. Nonferr Met Sci Eng 4(2):8–13. https://doi.org/10.13264/j.cnki.ysjskx.2013.02.015
25. Ye L, Tang C, Liu H, Chen Y (2019) Efficient bath-smelting reduction of antimony oxide in FeO–SiO_2–CaO–Na_2O quaternary slag with low melting point. JOM 71(11):3903–3908. https://doi.org/10.1007/s11837-018-3262-9
26. Yu-Jie H, Chao-Bo T, Mo-Tang T, Yong-Ming C (2015) Reductive smelting of spent lead–acid battery colloid sludge in a molten Na_2CO_3 salt. Int J Miner Metall Mater 22:798–803. https://doi.org/10.1007/s12613-015-1136-5
27. Chen P, Xiao H, Chen J, Chen L, Zhang D, Liu W, Yang T (2020) Oxygen-rich side-blown bath smelting of copper dross: a process. J Sustain Metall 6(2):344–354. https://doi.org/10.1007/s40831-020-00278-3
28. Dang X, Liu A, Lyu J (2018) Metal phase transformation and equilibrium distribution in sodium roasting process of the electroplating sludge. Chin J Environ Eng 12(10):2944–2951. https://doi.org/10.12030/j.cjee.201803085
29. Hidayat T, Shishin D, Decterov SA, Jak E (2017) Critical thermodynamic re-evaluation and re-optimization of the CaO–FeO–Fe_2O_3–SiO_2 system. CALPHAD 56:58–71. https://doi.org/10.1016/j.calphad.2016.11.009
30. Sridhar R, Toguri JM, Simeonov S (1997) Thermodynamic considerations in copper pyrometallurgy. JOM 49(4):48–52. https://doi.org/10.1007/bf02914876
31. Bale CW, Bélisle E, Chartrand P, Decterov SA, Eriksson G, Gheribi AE, Hack K, Jung IH, Kang YB, Melançon J, Pelton AD, Petersen S, Robelin C, Sangster J, Spencer P, Van Ende MA (2016) FactSage thermochemical software and databases, 2010–2016. CALPHAD 54:35–53. https://doi.org/10.1016/j.calphad.2016.05.002
32. Sridhar R, Toguri JM, Simeonov S (1997) Copper losses and thermodynamic considerations in copper smelting. Metall Mater Trans B 28(2):191–200. https://doi.org/10.1007/s11663-997-0084-5
33. Chen L, Yang T, Bin S, Liu W, Zhang D, Bin W, Zhang L (2014) An efficient reactor for high-lead slag reduction process: oxygen-rich side blow furnace. JOM 66(9):1664–1669. https://doi.org/10.1007/s11837-014-1057-1
34. Nikolic S, Hayes PC, Jak E (2008) Phase equilibria in ferrous calcium silicate slags: Part IV. Liquidus temperatures and solubility of copper in "Cu_2O"–FeO–Fe_2O_3–CaO–SiO_2 slags at 1250°C and 1300°C at an oxygen partial pressure of 10^{-6} atm. Metall Mater Trans B 39(2):210–217. https://doi.org/10.1007/s11663-008-9129-7
35. Shishin D, Shevchenko M, Jak E (2021) Experimental study and thermodynamic calculations in the CaO–Cu_2O–FeO–Fe_2O_3–SiO_2 system for applications in novel copper-based processes. J Sustain Metall 7:300–313. https://doi.org/10.1007/s40831-021-00341-7
36. Sukhomlinov D, Avarmaa K, Virtanen O, Taskinen P, Jokilaakso A (2020) Slag–copper equilibria of selected trace elements in black copper smelting. Part I. Properties of the slag and chromium solubility. Miner Process Extr Metall Rev 41(1):32–40. https://doi.org/10.1080/08827508.2019.1575212
37. Ilyushechkin A, Hayes PC, Jak E (2014) Effects of Al_2O_3, CaO and Cr_2O_3 on liquidus temperatures of Fe–Mg–Si–O slags. Can Metall Q 54(2):185–197. https://doi.org/10.1179/1879139514y.0000000177
38. Mäkinen T, Taskinen P (2013) State of the art in nickel smelting: direct Outokumpu nickel technology. Miner Process Extr Metall 117(2):86–94. https://doi.org/10.1179/174328508X290867
39. Bates C, Dimartini C (1986) Sodium treatment of copper dross. JOM 38(8):43–45. https://doi.org/10.1007/bf03257788
40. Chen L, Chen P, Wang Z, Liu W, Zhang D, Yang T (2021) Selective reduction of lead sulfate containing slag using the fluidized bed reactor. J Clean Prod 296:126512. https://doi.org/10.1016/j.jclepro.2021.126512
41. Chen W, Mei C (1993) A handbook for extractive metallurgy of nonferrous metals—modern equipments. Metallurgical Industry Press, Beijing
42. State Environmental Protection Administration of China (2007) Identification standards for hazardous wastes—identification for extraction toxicity. http://openstd.samr.gov.cn/bzgk/gb/newGbInfo?hcno=186B648DFF1A74025E1AA0117DFE3917. Accessed 2 Mar 2022
43. Code of Federal Regulations (2022) 261.24 Toxicity characteristic. https://www.ecfr.gov/current/title-40/chapter-I/subchapter-I/part-261/subpart-C/section-261.24. Accessed 4 Mar 2022
44. United States Environmental Protection Agency (2022) SW-846 test method 1311: toxicity characteristic leaching procedure. https://www.epa.gov/hw-sw846/sw-846-test-method-1311-toxicity-characteristic-leaching-procedure. Accessed 4 Mar 2022
45. Ivan K, Slavica Z, Vesna L, Miodrag S, Tatjana G (2018) Use of sintering to immobilize toxic metals present in galvanic sludge into a stabile glass–ceramic structure. Sci Sinter 50(2):139–147. https://doi.org/10.2298/SOS1802139K